CHEMISTRY
A European Journal

Supporting Information

Spectral Signatures of Ultrafast Spin Crossover in Single Crystal $[Fe^{II}(bpy)_3](PF_6)_2$

Ryan Field,[a, b] Lai Chung Liu,[a, b] Wojciech Gawelda,[c] Cheng Lu,[a] and R. J. Dwayne Miller*[a, b]

chem_201600374_sm_miscellaneous_information.pdf

Experimental Methods:

All chemicals were purchased from Sigma-Aldrich Company and were used without further purification. The acetonitrile solvent (CH_3CN) was dried and freshly distilled under nitrogen prior to use.

For the preparation of tris(bipyridine)iron(II) chloride ($[Fe^{II}(bpy)_3]Cl_2$), a CH_3CN solution of 2,2'-bipyridine was added to an aqueous solution of iron(II) chloride tetrahydrate. The mixture was gently heated to 70˚C, and stirred for 2 hours. After an additional filtration, the solution was dried in vacuum and the dry residuum was dissolved and recrystallized in CH_3CN. In order to exchange chloride counterions with hexafluorophosphate ions (PF_6^-), an aqueous solution of chloride salt was added to an aqueous solution of NH_4PF_6 and stirred at room temperature for 0.5 h. The solid compound that formed was filtered, dried in air, and then recrystallized from CH_3CN.

Single crystals of $[Fe^{II}(bpy)_3](PF_6)_2$ of varying thickness (~100–300 nm) were microtomed along the (210) plane and loaded on 0.5 mm thick sapphire substrates for measurement. The cleaved 2D membranes used in the transient absorption (TA) scans shown had an approximate thickness of 200 nm unless otherwise noted. Aqueous samples were prepared by dissolving $[Fe^{II}(bpy)_3]Cl_2$ in deionized water and measured in a 400 μm thick flow cell with 150 μm thick quartz windows.

The pump and probe pulses used for transient absorption measurements were generated using a fraction of the output from a commercial regenerative amplifier system (Coherent Legend). This system outputs 3.5 mJ, ~40 fs pulses centered at 800 nm at a repetition rate of 1 kHz.

The broadband probe pulses were generated using the scheme similar to that presented by Johnson et al.[1] Briefly, a small fraction of the fundamental was circularly polarized using a quarter-wave plate and then focused into a 2 mm thick CaF_2 plate that was kept under rotation to prevent damage. The generated supercontinuum, which retains the circular polarization of the seed, was collimated using an off-axis parabolic mirror and then returned to a linear polarization state using an achromatic quarter-wave plate, which was also used to set the polarization of the probe relative to the crystal axis of the sample. An optical filter was used to remove the residual seed light. For the UV experiments, the fundamental was frequency doubled in a 1 mm thick 29.5° cut β-barium borate (BBO) crystal prior to the quarter-wave plate (with the quarter-wave plates and filter replaced with ones appropriate to the wavelength range). This allowed us to extend the supercontinuum into the UV. In both cases, the energy of the seed pulses was set using a half-wave plate and polarizing beam splitter.

The 400 nm pump pulses were generated by frequency doubling the fundamental in a 0.2 mm thick 29.2° cut BBO crystal. The pump was then passed through a 4F acousto-optic pulse shaper[2,3] to compress the pulses to near the transform limit, and to provide fine control of the pulse energy. A half-wave plate was placed after the shaper to control the polarization of the pump. A transient-grating frequency-resolved optical gating spectrometer (TG FROG) was used to characterize the pump pulse duration, which was found to be 53 fs.

At the sample position, the pump and probe beams were focused to an approximate $1/e^2$ diameter of 90 μm and 60 μm respectively, using all-reflective optics to prevent additional chirp in the pulses. For the single crystal measurements, parallel pump and probe polarizations were used, with the probe polarization set to maximize the sample absorption at 533 nm. For measurements on the aqueous solution, the pump and probe polarizations were set at the magic angle. The pump fluence at the sample position was approximately 3 mJ cm^{-2} (corresponding to a pulse energy of 100 nJ) unless otherwise noted, which is within the range where the TA response is linear (see Figure S1). The estimated instrument response times (FWHM) are (81 ± 9) fs and (90 ± 11) fs in the UV and visible ranges, respectively. The delay

between the pump and probe pulses was controlled using a motorized translation stage with a minimum travel of 100 nm.

The spectrum of the probe pulse was resolved using a home-built spectrometer. The spectrometer used a 300 grooves mm^{-1}, 2°34' blaze angle reflection grating to disperse the spectrum, which was then focused on a 2048 pixel CCD array. An optical chopper was used to block or pass four adjacent pump pulses for the "pump-off" and "pump-on" spectra, respectively. The measured signal was integrated over these four spectra for each chopper state, and the resultant differential absorption spectrum was averaged 200 times at each delay step. The averaged spectrum was smoothed over five adjacent pixels using a moving average (corresponding to a range of approximately 0.7 nm). Some of the TA scans used have had the spectra recorded at a small number of delay points (<10) removed, typically because of incorrectly recorded chopper phase, and replaced with linear interpolations from the neighbouring delay points. The magnitude of the dA signal was normalized to variations in the pump intensity measured from a weak reflection off a fused silica window in the pump beam path using a slow photodiode. Ground state absorption spectra were measured in situ by measuring the probe spectrum transmitted through the sample at the position probed in the TA measurements, then through a blank (sapphire or water in the crystal and aqueous experiments, respectively).

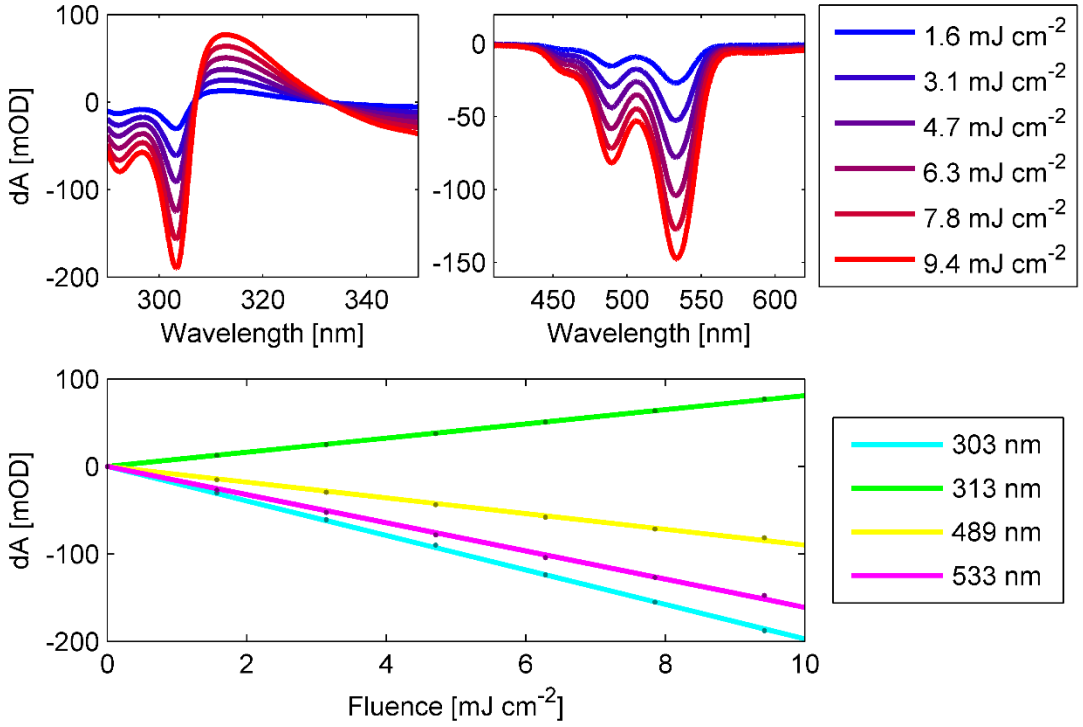

Figure S1: Top: UV and visible TA spectra at 5 ps after excitation of $[Fe^{II}(bpy)_3](PF_6)_2$ single crystals using various pump fluences. These spectra are taken from raw data and have not been corrected for group velocity dispersion of the probe. Bottom: Linear fits of TA at selected wavelengths as a function of pump fluence, demonstrating the linearity of the signal. Beyond the range of fluences shown (greater than approximately 10 mJ cm^{-2} fluence or 200 GW cm^{-2} intensity) damage was found to occur to the samples. This manifested as an irreversible change to the TA spectrum, and visible distortions to the spatial profiles of the transmitted pump and probe beams.

Method of Analysis:

Group velocity dispersion (GVD) causes a different measured t = 0 delay at each wavelength across the probe window. The t = 0 delays were estimated using the cross-phase modulation (CPM) signal

measured in deionized water in a flow cell or a sapphire substrate for the aqueous and single crystal measurements respectively, using the same excitation conditions as in the measured TA scans.

At each wavelength, the measured time-trace of the CPM was convoluted with its mirror image. The resulting trace was fitted with a Gaussian whose center was taken as the t = 0 delay. The GVD was then corrected by shifting each time trace to align the estimated t = 0 delay with the global minimum. Shifts whose magnitude were less than the time-step of the measurement were achieved through spline interpolation. The shifts estimated by this method were then applied to the corresponding aqueous $[Fe^{II}(bpy)_3]^{2+}$ and single crystal $[Fe^{II}(bpy)_3](PF_6)_2$ TA scans. GVD correction was not applied to the long time-delay scans.

The instrument response function (IRF) was assumed to be Gaussian. To estimate the instrument response time, the CPM measured in water was fitted at each wavelength with a Gaussian and its first four derivatives. The FWHM of the Gaussians used in the fit were averaged across all wavelengths to give the estimated instrument response time. The standard deviation of the Gaussian widths was taken as the error to reflect the variation of the instrument response across the probe window.

Following the correction of the GVD and estimation of the instrument response time, the data presented were analyzed using global analysis (GA), wherein all the observations in the time-wavelength plots were fitted simultaneously with a small number of spectral components and associated kinetic traces.[4] The end result of this analysis is to describe the full data set with a small number of decay associated spectra (DAS) with associated exponential decay rates. As this analysis only describes exponential dynamics, the non-exponential dynamics (oscillatory in this case) appear in the residuals.

The analysis proceeded first by means of a singular value decomposition (SVD). This decomposition allows us to greatly reduce the dimensionality of the data, and gives the basis spectra and kinetic traces from which the global fit was generated. For an M × N data matrix, Ψ (in this case corresponding to M wavelength points and N time points), the SVD is given by

$$\Psi = USV^T \tag{S1}$$

where U and V are orthogonal matrices of size M × M and N × N, whose columns are the left and right singular vectors, respectively. S is an M × N diagonal matrix which contains the singular values, s_j, on the diagonal. In the following analysis, the left and right singular vectors were taken as basis spectra and kinetic traces. The kinetic traces were fitted using the function described below, and the resulting fit values were used along with the basis spectra to construct a global fit.

Our analysis assumes kinetic behaviour that can be described by a sum of Q exponential decays convoluted with the IRF, which was assumed to be a Gaussian centered at t = 0.[4,5] This describes the analytical function given by:

$$E(t) = \frac{1}{2}\sum_{i=1}^{Q} a_i \exp\left[-k_i t + \frac{(k_i\sigma)^2}{2}\right]\left[1 + \operatorname{erf}\left(\frac{t - k_i\sigma^2}{\sqrt{2}\sigma}\right)\right] \tag{S2}$$

where a_i and k_i are the amplitude and decay rate of the ith component, respectively, and σ is the width of the IRF. Additionally, to fit the contribution from the CPM, a function consisting of the sum of a Gaussian (with width σ, centered at t=0) and its first four derivatives was added to the fit function:

$$C(t) = \sum_{n=0}^{4} b_n \frac{(-1)^n}{\sqrt{2^n n!}} \exp\left[-\frac{1}{2}\left(\frac{t}{\sigma}\right)^2\right] \frac{d^n}{dt^n} \exp\left[-\frac{1}{2}\left(\frac{t}{\sigma}\right)^2\right] \tag{S3}$$

where b_n is the amplitude of nth term, and σ is the width of the IRF, as above. The normalization prefactors were used so that the terms in the sum form an orthogonal basis set. This part of the fit was not used in reconstructing the global fit, but was rather used to give better estimation of exponential decays with rates on the same order as the instrument response time.

To construct the global fit, all of the significant kinetic traces (V_l^T for the lth trace) were fitted simultaneously to the function:

$$F_l(t) = E_l(t) + C_l(t) \tag{S4}$$

Each of these fits used shared decay rates, k_i, but independent amplitudes $a_{i,l}$ and $b_{n,l}$. The CPM term was not used in fitting the long time-delay scans, as it does not contribute significantly to the signal within the time resolution of those measurements.

A decay-associated spectra (DAS_i) was calculated for each decay rate. Each DAS was calculated as a linear combination of the basis spectra, U_l, weighted by its corresponding singular value, s_l, and by each of the $a_{i,l}$ amplitudes, according to:[4]

$$DAS_i = \sum_{l=1}^{Q} a_{i,l}\, s_l U_l \tag{S5}$$

Finally, the global fit was calculated for each time point by summing the product of each of the DAS and the kinetic trace for the corresponding decay rate:

$$GA(t) = \sum_{i=1}^{Q} DAS_i \exp\left[-k_i t + \frac{(k_i\sigma)^2}{2}\right]\left[1 + \mathrm{erf}\left(\frac{t - k_i\sigma^2}{\sqrt{2}\sigma}\right)\right] \tag{S6}$$

The residuals of the fit primarily reflect the CPM and the oscillatory dynamics. To extract the relevant frequencies, the residuals for delay times after t = 300 fs were Fourier transformed at each wavelength. The transformed residuals were then integrated over all wavelengths. The significant peaks in the integrated transform were fitted with Gaussians to extract the peak centers and error bars. The error bars represent the FWHM of the Gaussians used in the fit.

Supplementary Single Crystal $[Fe^{II}(bpy)_3](PF_6)_2$ Results:

The residuals of the fit used for the TA scan shown in Figure 2 of the main text are shown in Figure S2. The residuals primarily reflect the CPM and the oscillatory dynamics.

The period of the oscillations seen in the residuals of the long time-delay scan in the visible range was found to vary linearly with the optical density (and therefore thickness) of the crystal sample used. The measured optical density at the 533 nm peak and the oscillation period of multiple samples with varying thickness (~100–300 nm thick) are shown in Figure S3, along with a linear fit where the y-intercept is fixed at zero.

A comparison between the DAS extracted from the fit of the long time-delay visible TA scans and the measured ground state absorption spectrum and its second derivative are shown in Figure S4. The agreement between the 98 ps DAS and the ground state (GS) absorption shows that this component primarily reflects the recovery of the GS. The effectively infinite DAS shows good correspondence in the peak positions and signs with the second derivative of the GS absorption, although the relative magnitudes of the peaks differ. We interpret the process represented by this component as transient heating of the crystal lattice.

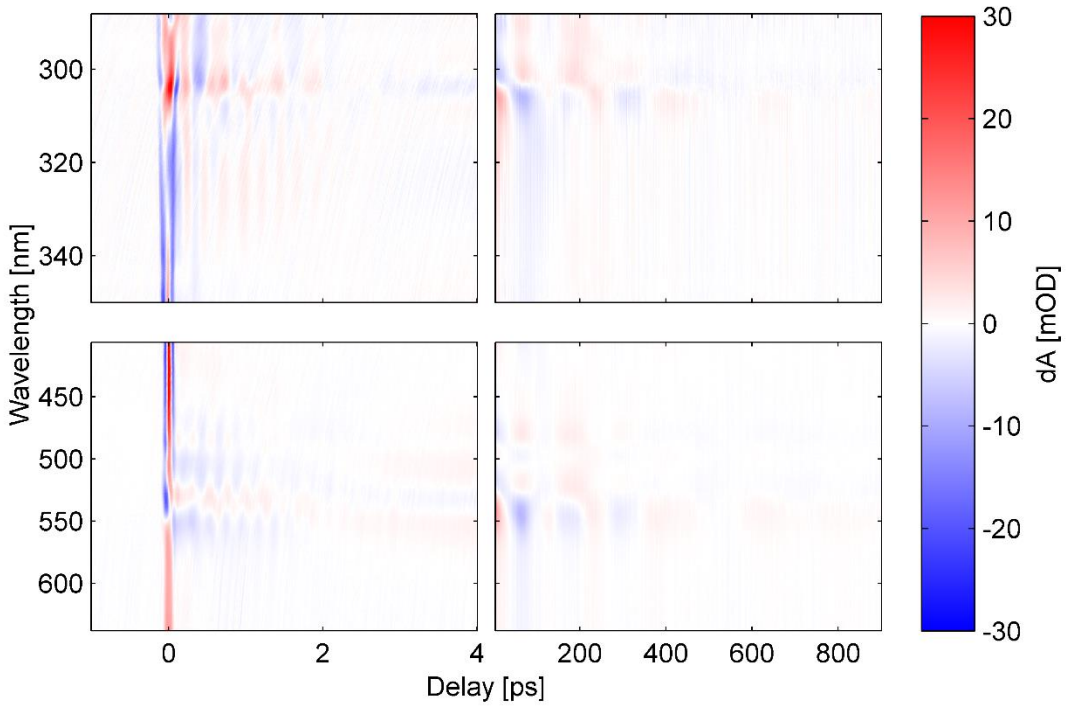

Figure S2: Residuals of the global fits shown in Figure 2 of the main text.

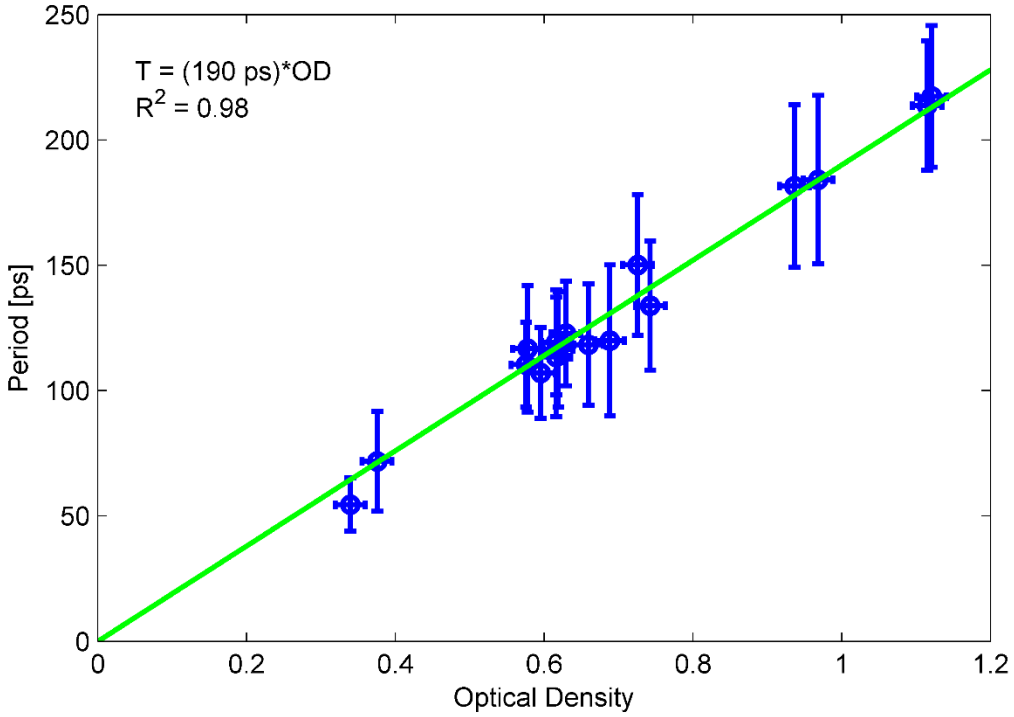

Figure S3: Sample optical density vs. period for the oscillations observed in the long time-delay scans in the visible range. T is period and OD is optical density.

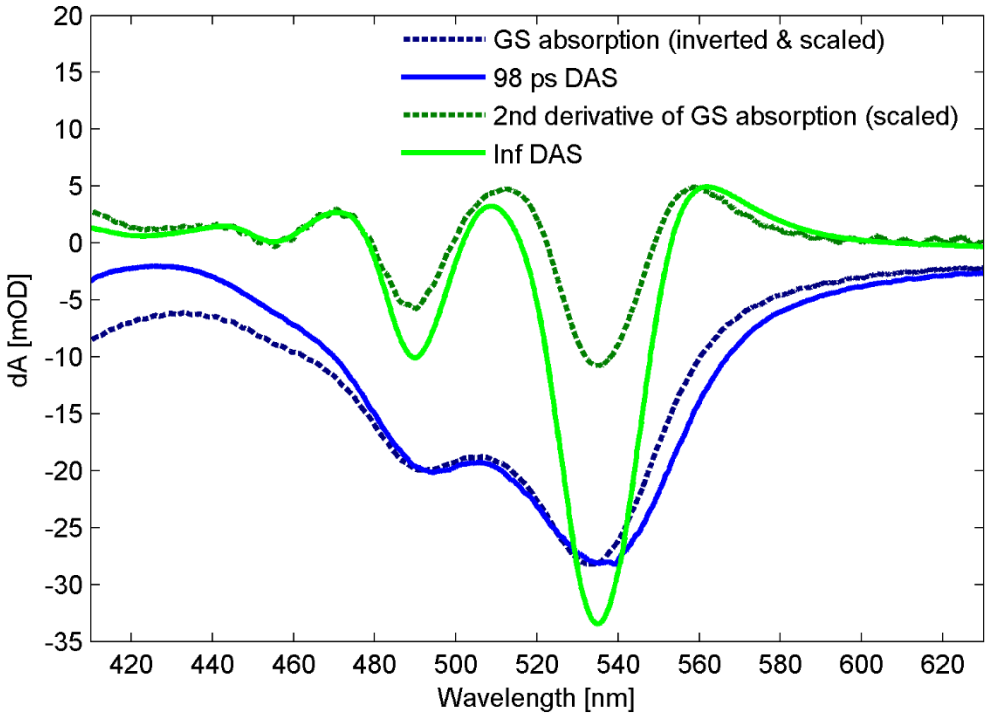

Figure S4: Comparison of the GS absorption spectrum and its second derivative to the DAS used in the fit of the visible long time-delay scan shown in Figure 2 of the main text.

Aqueous $[Fe^{II}(bpy)_3]^{2+}$ Control Experiment:

As a control experiment for the crystal studies presented in the main text, we have measured and analyzed TA scans of aqueous $[Fe^{II}(bpy)_3]^{2+}$ under similar excitation conditions as those used in the single crystal studies. The measured data is shown in Figure S5.

In the visible region, the TA is dominated by a negative change in absorptivity corresponding to ground state bleach (GSB). Additionally, there is a short-lived positive component apparent at wavelengths <460 nm and >550nm. This has previously been attributed to excited state absorption (ESA) of the MLCT state.[5,6] In the UV region, strong ESA is observed at wavelengths <335 nm, with a negative GSB contribution at higher wavelengths. This ESA has been attributed to the absorption of the $^5T_2$ HS state.[6,7] Additionally, there is apparent narrowing and blue shifting of the HS signal, which has been attributed to cooling of the vibrationally hot HS state. At early times, oscillations are present in the HS ESA, as well as in the GSB in the visible range. The GSB and HS ESA signals persist over several hundred picoseconds, as seen in the long time-delay scans.

Applying the GA used on the crystal samples to this data set reveals similar behaviour. The resulting fits are shown in Figure S6 and the corresponding DAS are shown in Figure S7. The early-time data in the visible is fitted with two components. The short component has a lifetime of (86 ± 5) fs, which is comparable to the instrument response time. This component reflects the decay of the short-lived MLCT absorption at wavelengths <460 nm and >550nm. The second component, which is effectively infinite on this time scale, represents the contribution of the GSB. The long time-delay scan in this

wavelength range can be fitted with a single component which decays in (699 ± 12) ps and is due to the HS→LS relaxation.

The UV data at early times are fitted with 3 spectral components. The shortest component has a lifetime of (62 ± 29) fs, and describes the decay of the short-lived MLCT seen at t <100 fs and the rise of the ESA band at wavelengths <335 nm. This band, along with the long-lived GSB at wavelengths >335 nm are described by a component which is effectively infinite on this time scale. Additionally, a component with a (1.4 ± 0.1) ps lifetime reflects the blue-shifting of the long-lived HS ESA band. The long time-delay scan can again be fitted with a single component which decays in (645 ± 6) ps, although this leaves a slight residual at t < 6 ps corresponding to the blue-shifting of the HS ESA band, which is not well resolved on this time scale. The (645 ± 6) ps component can be interpreted as the HS→LS transition.

A single (128 ± 13) cm^{-1} mode was extracted from the Fourier transform of the residuals of the UV scan (Figure S9). This was also observed in the visible range, albeit with a much lower amplitude. This mode has been observed previously and was attributed to a wavepacket on the HS surface resulting from an Fe–N stretching or bending mode.[6,7] Other modes reported in [6] may have been present but were not clearly resolvable above the noise level.

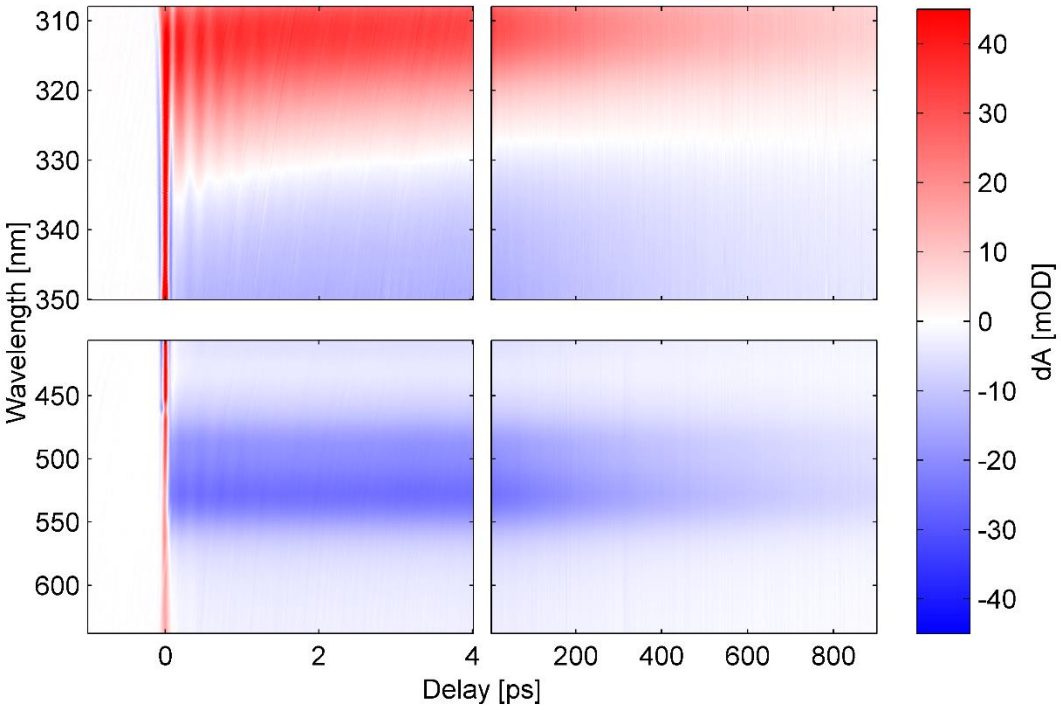

Figure S5: Transient-absorption scans of aqueous $[Fe^{II}(bpy)_3]^{2+}$ in the UV (top) and visible (bottom) regions. Short (-1–4 ps) and long (4–900 ps) time scales are shown, using 10 fs and 2 ps delay steps, respectively.

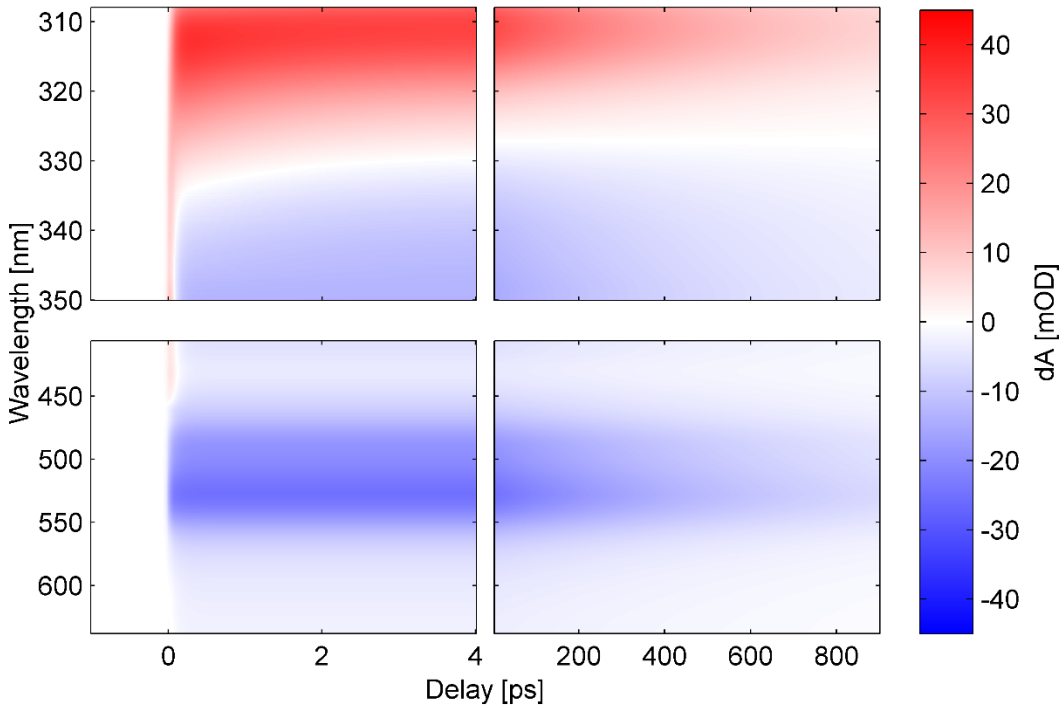

Figure S6: Results of the global fit in the UV (top) and visble (bottom) regions applied to the data presented in Figure S5.

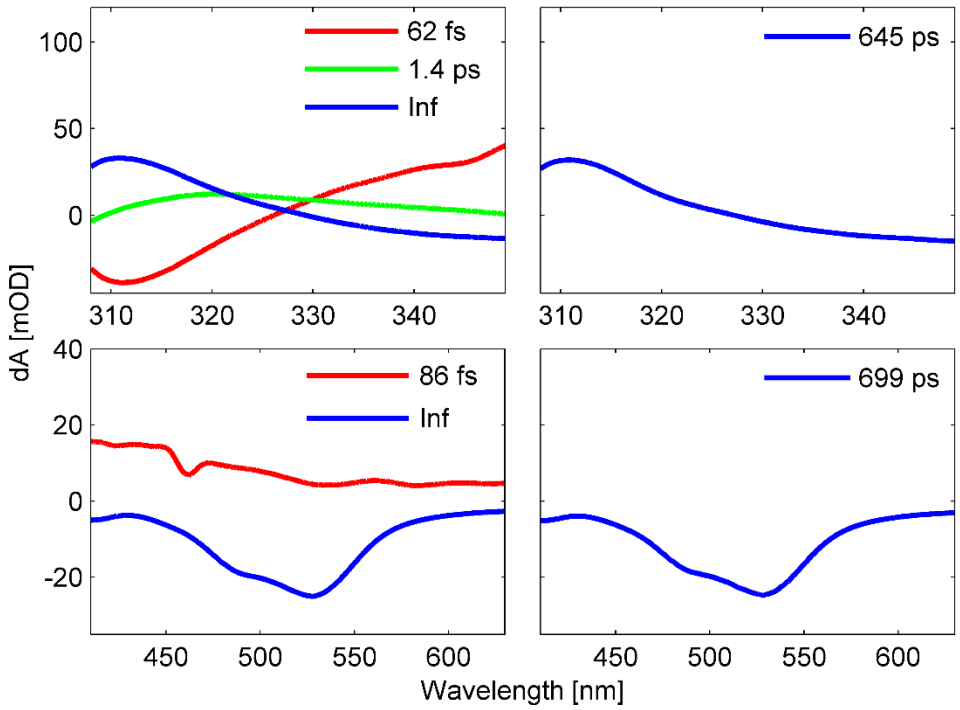

Figure S7: Decay associated spectra used in the fits shown in figure S6. The DAS are shown for the short (left) and long (right) time-delay scans.

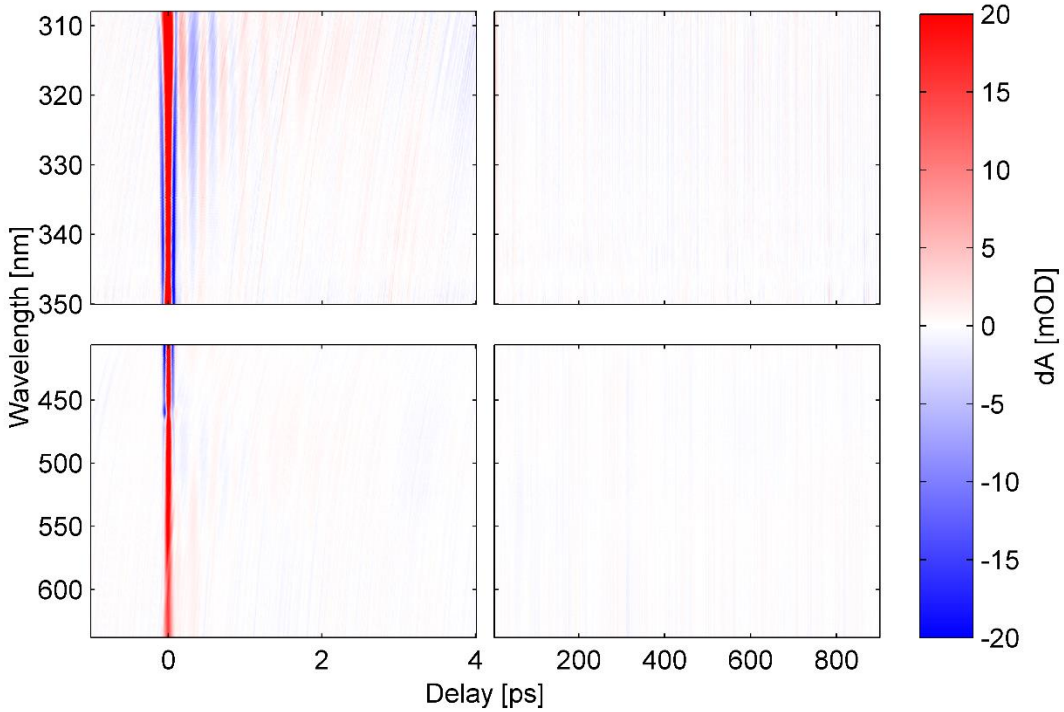

Figure S8: Residuals of the global fits shown in Figure S6.

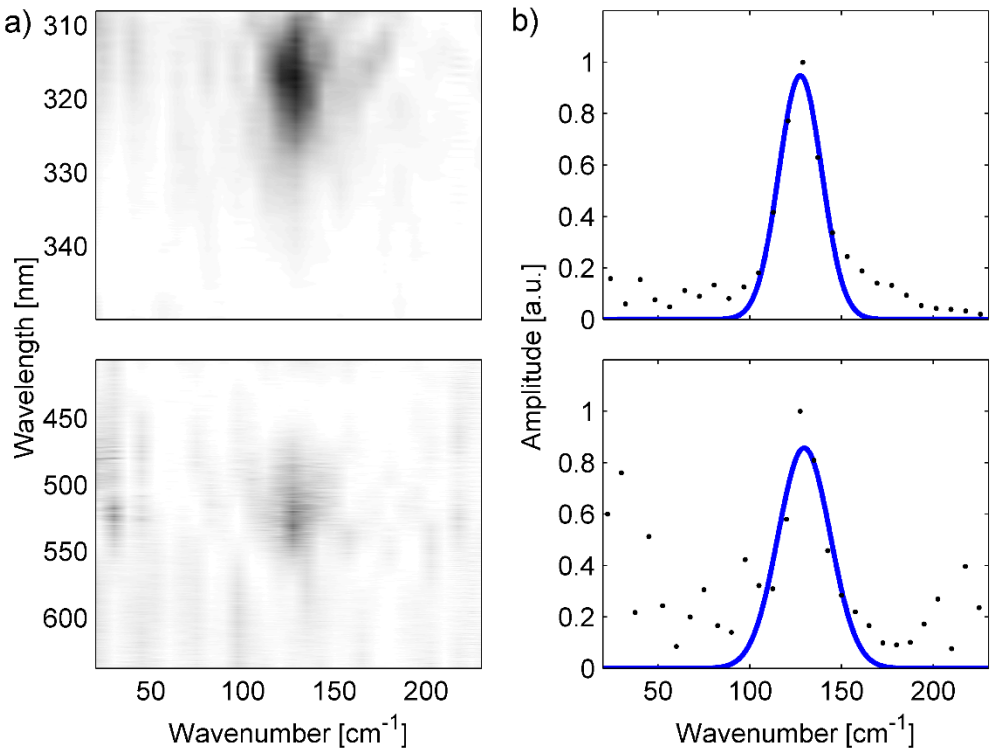

Figure S9: a) Spectrally resolved Fourier transforms of the aqueous data's global fit's residuals in the UV (top) and visible (bottom) ranges. For visual clarity, the visible range data is multiplied by 10. b) Spectrally integrated Fourier transforms with Gaussian fits in the UV (top) and visible (bottom) ranges.

Table T1: Parameters used to fit the kinetic traces (V_l) from the SVD of the $[Fe^{II}(bpy)_3](PF_6)_2$ single crystal data.

	Decay Associated Amplitudes			**CPM Amplitudes**				
UV Short Scan (σ = 32 fs, fixed)	k_1 = 3.895×10^{-14} fs^{-1} (Inf)	k_2 = 9.271×10^{-3} fs^{-1}	k_3 = 5.930×10^{-4} fs^{-1}					
	a_1	a_2	a_3	b_0	b_1	b_2	b_3	b_4
V_1	0.048	-0.012	0.001	-0.021	-0.008	-0.006	-0.005	-0.000
V_2	-0.053	0.273	0.142	-0.174	-0.052	-0.131	0.071	-0.019
V_3	-0.026	-0.518	0.089	-0.048	0.116	0.154	0.043	0.171
UV Long Scan (σ = 32 fs, fixed)	k_1 = 0.714×10^{-7} fs^{-1} (Inf)	k_2 = 1.001×10^{-5} fs^{-1}						
	a_1	a_2	a_3	b_0	b_1	b_2	b_3	b_4
V_1	-0.042	-0.047						
V_2	0.035	-0.220						
Vis Short Scan (σ = 34 fs, fixed)	k_1 = 1.000×10^{-7} fs^{-1} (Inf)	k_2 = 1.390×10^{-2} fs^{-1}						
	a_1	a_2	a_3	b_0	b_1	b_2	b_3	b_4
V_1	0.046	0.008		-0.002	-0.011	0.013	0.002	-0.002
V_2	0.003	-0.276		-0.198	-0.012	0.254	0.041	-0.078
Vis Long Scan (σ = 34 fs, fixed)	k_1 = 0.998×10^{-7} fs^{-1} (Inf)	k_2 = 1.017×10^{-5} fs^{-1}						
	a_1	a_2	a_3	b_0	b_1	b_2	b_3	b_4
V_1	0.042	0.050						
V_2	-0.037	0.2233						

Table T2: Parameters used to fit the kinetic traces (V_i) from the SVD of the aqueous $[Fe^{II}(bpy)_3]^{2+}$ data.

	Decay Associated Amplitudes			**CPM Amplitudes**				
UV Short Scan (σ = 32 fs, fixed)	k_1 = 1.000 × 10^{-7} fs^{-1} (Inf)	k_2 = 1.604 × 10^{-2} fs^{-1}	k_3 = 7.113 × 10^{-4} fs^{-1}					
	a_1	a_2	a_3	b_0	b_1	b_2	b_3	b_4
V_1	-0.044	0.059	-0.011	-0.051	-0.001	-0.014	0.005	0.009
V_2	-0.020	0.105	0.047	0.312	-0.043	-0.158	-0.009	-0.074
V_3	-0.048	-0.098	0.167	-0.160	0.121	-0.056	0.024	-0.112
UV Long Scan (σ = 32 fs, fixed)	k_1 = 1.550 × 10^{-6} fs^{-1}							
	a_1	a_2	a_3	b_0	b_1	b_2	b_3	b_4
V_1	-0.082							
Vis Short Scan (σ = 34 fs, fixed)	k_1 = 2.337 × 10^{-14} fs^{-1} (Inf)	k_2 = 1.158 × 10^{-2} fs^{-1}						
	a_1	a_2	a_3	b_0	b_1	b_2	b_3	b_4
V_1	0.046	-0.020		-0.068	-0.004	0.025	-0.001	-0.006
V_2	0.005	0.146		0.249	0.046	-0.230	-0.024	0.083
Vis Long Scan (σ = 34 fs, fixed)	k_1 = 1.430 × 10^{-6} fs^{-1}							
	a_1	a_2	a_3	b_0	b_1	b_2	b_3	b_4
V_1	0.079							

References:

[1] P. J. M. Johnson, V. I. Prokhorenko, R. J. D. Miller, *Opt. Express* **2009**, 17, 21488

[2] C. W. Hillegas, J. X. Tull, D. Goswami, D. Strickland, W. S. Warren, *Opt. Lett.* **1994**, 19, 737

[3] M. Roth, M. Mehendale, A. Bartlet, H. Rabitz, *Appl. Phys. B* **2005**, 80, 441

[4] I. H. M. van Stokkum, D. S. Larsen, R. van Grondelle, *Biochim. Biophys. Acta* **2004**, 1657, 82

[5] W. Gawelda, A. Cannizzo, V. T. Pham, F. van Mourik, C. Bressler, M. Chergui, *J. Am. Chem. Soc.* **2007**, 129, 8199.

[6] G. Auböck, M. Chergui, *Nat. Chem.* **2015**, 7, 629

[7] C. Consani, M. Prémont-Schwarz, A. ElNahhas, C. Bressler, F. van Mourik, A. Cannizzo, M. Chergui, *Angew. Chem. Int. Ed.* **2009**, 48, 7184; *Angew. Chem.* **2009**, 121, 7320.